DR. TOBIAS GABRIEL BOATMAN (Orcid ID : 0000-0001-7541-3844)

Article type : Primary Research Articles

# Projected expansion of *Trichodesmium's* geographical distribution and increase of growth potential in response to climate change

Running Head: ***Trichodesmium's* fundamental niche**

TOBIAS G. BOATMAN[1], GRAHAM J.G. UPTON[2], TRACY LAWSON[1], RICHARD J. GEIDER[1]

[1] School of Life Sciences, University of Essex, Colchester, CO4 3SQ, UK

[2] Department of Mathematical Sciences, University of Essex, Colchester, CO4 3SQ, UK

Correspondence: Tobias G Boatman, toby@susewi.life

Keywords: *Trichodesmium*, Cyanobacteria, Ocean acidification, Sea Surface Temperature, $CO_2$, Fundamental niche

This article has been accepted for publication and undergone full peer review but has not been through the copyediting, typesetting, pagination and proofreading process, which may lead to differences between this version and the Version of Record. Please cite this article as doi: 10.1111/GCB.15324

Primary Research Article

**Abstract**

Estimates of marine $N_2$ fixation range from 52 to 73 Tg N $yr^{-1}$, of which we calculate up to 84% is from *Trichodesmium* based on previous measurements of *nif*H gene abundance and our new model of *Trichodesmium* growth. Here we assess the likely effects of four major climate change-related abiotic factors on the spatiotemporal distribution and growth potential of *Trichodesmium* for the last glacial maximum (LGM), the present (2006-2015) and the end of this century (2100) by mapping our model of *Trichodesmium* growth onto inferred global surface ocean fields of $pCO_2$, temperature, light and Fe. We conclude that growth rate was severely limited by low $pCO_2$ at the LGM, that current $pCO_2$ levels do not significantly limit *Trichodesmium* growth and thus, the potential for enhanced growth from future increases of $CO_2$ is small. We also found that the area of the ocean where sea surface temperatures (SST) are within *Trichodesmium's* thermal niche increased by 32% from the LGM to present, but further increases in SST due to continued global warming will reduce this area by 9%. However, the range reduction at the equator is likely to be offset by enhanced growth associated with expansion of regions with optimal or near optimal Fe and light availability. Between now and 2100, the ocean area of optimal SST and irradiance is projected to increase by 7%, and the ocean area of optimal SST, irradiance and iron is projected to increase by 173%. Given the major contribution of this keystone species to annual $N_2$ fixation and thus pelagic ecology, biogeochemistry and $CO_2$ sequestration, the projected increase in the geographical range for optimal growth could provide a negative feedback to increasing atmospheric $CO_2$ concentrations.

**Keywords:** *Trichodesmium*, Cyanobacteria, Ocean acidification, $CO_2$, Sea surface temperature, Fundamental niche, Growth potential

## Introduction

Marine phytoplankton account for about 45% of global net primary production (Field *et al.*, 1998), and as such play an important role in the global carbon cycle (Arrigo, 2007). Approximately 20% of the annual marine net primary production is exported from the surface to the deep via sinking particles (Buesseler & Boyd, 2009). This export production contributes to the draw-down of $CO_2$ from the atmosphere and its sequestration for hundreds or thousands of years in the deep ocean. Maintaining net primary production requires a source of fixed N (e.g. ammonium, nitrite, nitrate and organic N) which can be supplied to the euphotic region by mixing and upwelling of nitrate from the deep, deposition of nitrate and organic N from the atmosphere and $N_2$ fixation by diazotrophic cyanobacteria (Duce *et al.*, 2008).

Nitrogen fixation accounts for more than half of the export of organic carbon from the surface ocean to the deep ocean in some parts of the oligotrophic tropical and subtropical oceans (Capone, 2005), and is likely to be 2-3 times more important than the atmospheric delivery of fixed N to the sea (Duce *et al.*, 2008). Changes in export production could significantly affect the ocean's ability to sequester $CO_2$ from the atmosphere and store it in the deep ocean. When operating over geological timescales, for example, between glacial and interglacial periods, even small changes in the balance between $N_2$ fixation and the loss of fixed N due to denitrification can significantly affect the amount of $CO_2$ that can be stored in the ocean (Falkowski & Raven, 1997, Kohfeld & Ridgwell, 2009).

One manifestation of global warming is the increase of sea surface temperature (SST), which enhances water stratification and leads to the expansion of hot tropical and warm subtropical regions (Doney *et al.*, 2007). Although the reduced flux of nitrate into the upper mixed layer associated with increased stratification will be detrimental to many phytoplankton groups, the expansion of these nitrogen-limited regions may give diazotrophic cyanobacteria like *Trichodesmium* a competitive advantage and accentuate competition for other limiting nutrients (e.g. Fe or P). Alongside global warming, increasing atmospheric $CO_2$ is driving increases in seawater $CO_2$ concentrations, lowering pH and changing the inorganic carbon (Rost *et al.*, 2008)

and iron chemistry (Millero, 2009, Shi *et al.*, 2010, Shi *et al.*, 2007), all of which will have consequences for the structure and functioning of marine ecosystems.

Various explanations have been proposed for how future global change may affect *Trichodesmium* abundance and productivity. Breitbarth *et al.* (2007) suggest that *Trichodesmium's* fundamental niche will be principally determined by the direct physiological relationship between abundance and SST. Other research suggests that $CO_2$ concentrations projected for the end of this century (~720/750 ppm $CO_2$) could enhance rates of photosynthesis, nitrogen fixation and growth of *Trichodesmium* (Barcelos e Ramos *et al.*, 2007, Boatman *et al.*, 2017, Boatman *et al.*, 2018c, Hutchins *et al.*, 2007, Levitan *et al.*, 2007). In contrast, Monteiro *et al.* (2011) concluded that *Trichodesmium's* niche will be constrained at higher latitudes due to the loss of oligotrophic conditions and competition for nutrient resources. The generation and transport of Fe-containing dust into the ocean (Mahowald & Luo, 2003, Tegen *et al.*, 2004) will also affect the growth and productivity of *Trichodesmium* and other diazotrophs (Moore *et al.*, 2006). In addition, Jiang *et al.* (2018) have shown a temperature dependence of *Trichodesmium's* ability to assimilate Fe that in turn affects growth and nitrogen-fixation under Fe-limiting conditions.

To gain insight into changes in the distribution and growth potential of *Trichodesmium* from the last glacial maximum (LGM) to the present (2006-2015) and from the present to the end of this century, we combined information on how the growth of *Trichodesmium* responds to four key abiotic factors (temperature, $CO_2$, irradiance and iron availability) with inferred global surface ocean maps of these variables for these time periods.

## Materials and methods

### *Growth rate model*

The dependence of the steady state balanced growth rate of *Trichodesmium* on temperature, irradiance and iron was modelled as a multiplicative function:

$$\mu\,(\mathrm{d}^{-1}) = \mu_{max}{}'\left\{\sin\left[\pi\left(\frac{T-T_{min}}{T_{max}-T_{min}}\right)^{\theta}\right]\right\}^{\Phi}\left\{\frac{Fe'}{(K_m+Fe')}\right\}\left\{1-\exp\left(\frac{-E}{E_{k\alpha}}\right)\right\}\exp(-E\cdot E_{k\beta}) \qquad (1)$$

where $\mu_{max}{}'$ is the hypothetical maximum growth rate ($d^{-1}$) at the optimum temperature for growth before taking into account photoinhibition; T is the temperature (°C); $T_{min}$ and $T_{max}$ are the

minimum and maximum temperature limits for growth (°C); θ is a shape determining parameter which alters the skewness of the μ-T relationship; Φ is a shape determining parameter which alters the kurtosis of the μ-T relationship; Fe′ is the sum of inorganic iron complexes (Iron hydroxides + Fe(II)) (pM); $K_m$ is the half saturation concentration for Fe (pM); E is the irradiance (mol photons $m^{-2}$ $d^{-1}$); $E_{k\alpha}$ is the light saturation parameter (mol photons $m^{-2}$ $d^{-1}$); and $E_{k\beta}$ is the photoinhibition parameter (mol photons $m^{-2}$ $d^{-1}$).

The parameterisation of our *Trichodesmium* growth rate model was based on a series of long-term laboratory experiments (Boatman *et al.*, 2017, Boatman *et al.*, 2018c). In total, 184 treatments were cultured semi-continuously under well-defined growth conditions. Temperature (19 – 32 °C), irradiance (10 – 1400 μmol photons $m^{-2}$ $s^{-1}$), and iron-growth response curves were collected in parallel using identical methods and equipment and the data analysed using the same script-based code. All experiments consisted of a low (180 ppm), mid (380 ppm) and high (720 ppm) $CO_2$ treatment, as well as a low (40 μmol photons $m^{-2}$ $s^{-1}$) and high (400 μmol photons $m^{-2}$ $s^{-1}$) irradiance treatment (Fig. 1). A more detailed description of the laboratory methodology, culturing technique and analytical procedure is reported in our previous studies (Boatman *et al.*, 2017, Boatman *et al.*, 2018c).

As highlighted by Low‐Décarie *et al.* (2017), each equation was objectively selected based on the shape and data resolution of the growth response curves. The temperature response was modelled using a sine function (Boatman *et al.*, 2017), the light response using a two-phase exponential (initial slope and photoinhibition) function (Platt & Gallegos, 1980) and the Fe-response using a rate saturating function (Michaelis & Menten, 1913).

*Parameter optimisation*

Curve fitting to our multifactorial data set allowed growth rate to be modelled by specifying eight parameter values (Table S1); seven of which were independent of the $CO_2$, with one ($\mu_{max}'$) being $CO_2$ dependent. Curve fitting was performed on the median growth rate using a weighted non-linear least squares algorithm, where weights were the reciprocals of the standard errors associated with the growth rates. Initially, each $CO_2$ dataset (i.e. 180, 380 and 720 ppm) was modelled independently; producing three sets of parameterisations; each set consisting of 8 parameters

(Table S2). Then starting with $T_{min}$, data were combined between $CO_2$ datasets, and the model re-optimised. The data groupings consisted of i), combined low/mid $CO_2$ ii), combined low/high $CO_2$ iii), combined mid/high $CO_2$ and iv) all $CO_2$ data combined). Note, as previous studies have shown that *Trichodesmium's* maximum growth rate ($\mu_{max}$) is significantly reduced at low $CO_2$ relative to mid $CO_2$, and is consistently ~10% higher from mid to high $CO_2$ (Boatman *et al.*, 2018a, Boatman *et al.*, 2017, Boatman *et al.*, 2018b, Boatman *et al.*, 2018c), $\mu_{max}'$ was maintained independent between $CO_2$ conditions. Having processed all model iterations by optimising all parameter groupings, maximum likelihood ($L$) values were calculated using each model's residual sum of squares (RSS) and the number of data points ($n$ = 184). The best model (Model 29 in Table S2) consisted of seven global constants ($T_{min}$, $T_{max}$, $E_{k\alpha}$, $E_{k\beta}$, $\theta$, $\Phi$ and $K_m$) with one $CO_2$-dependent parameter ($\mu_{max}'$) (Table S1). Modelled against observed growth rates gave an $r^2$ value of 0.934 (Fig. S1).

*Modelled oceanographic data*

Mean monthly oceanographic data for sea surface chlorophyll (kg $m^{-3}$), temperature (SST) (°K), net downward radiation (W $m^{-2}$), dissolved iron (dFe) (mol $m^{-3}$) and mixed layer depth (MLD) (m) were obtained from the Institute Pierre Simon Laplace (IPSL), using the IPSL-CM5A-LR earth system model (Dufresne *et al.*, 2013). The data resolution was 1.875° x 3.75° with 39 vertical levels for the atmosphere and about 2° (with a meridional increased resolution of 0.5° near the equator) with 31 vertical levels for the ocean. All data files were transformed from a tripolar grid to a 180° x 360° latitudinal/longitudinal rectangular grid format, and interpolated to a 1-degree resolution.

Data files for the aforementioned variables were collected using the lgm and rcp60 experiment, where the lgm experiment yielded data for the last glacial maximum (LGM) while the rcp6.0 experiment yielded data for the present and future timescales. Mean monthly data files for each variable, at all three time periods, were averaged over a decade; present data was averaged between 2006-2015 and future data was averaged between 2091-2100. Based on the past, present and future climate emissions within the CM5A-LR lgm and rcp6.0 model, these time periods best match the low, mid and high $CO_2$ growth conditions of the laboratory experiments.

*Irradiance within the mixed layer*

Net downward radiation (W $m^{-2}$) was converted into a photosynthetic photon flux density (PPFD) by assuming half of the irradiance is photosynthetically active radiation (PAR) and that 1 W $m^{-2}$ of PAR is equivalent to a PPFD of 4.57 µmol photons $m^{-2}$ $s^{-1}$ (Langhans & Tibbitts, 1997). The mean PPFD within the mixed layer was calculated as follows (Helbling *et al.*, 1994):

$$E_z = E_0\left(\frac{1-\exp(-K_d(PAR)\cdot z)}{K_d(PAR)\cdot z}\right) \quad (2)$$

where $E_z$ is the mean PPFD within the mixed layer (µmol photons $m^{-2}$ $s^{-1}$), $E_0$ is the surface PPFD (µmol photons $m^{-2}$ $s^{-1}$), z is the MLD (m) and $K_d(PAR)$ is the light attenuation coefficient ($m^{-1}$) which was calculated using the Chl *a* data as follows (Dennison *et al.*, 1993):

$$K_d(PAR) = 0.121 \cdot Chl^{0.428} \quad (3)$$

The mean PPFD within the mixed layer was then converted into units of mol photons $m^{-2}$ $d^{-1}$ by calculating the photic period for each 1° longitudinal-latitudinal cell as follows:

$$D = 24 - \left(\frac{24}{\pi}\right)\cos^{-1}\left[\frac{\sin\frac{p\cdot\pi}{180} + \sin\frac{L\cdot\pi}{180}\sin\Phi}{\cos\frac{L\cdot\pi}{180}\cos\Phi}\right] \quad (4)$$

$$\Phi = \sin^{-1}[0.39795\cos\theta] \quad (5)$$

$$\theta = 0.2163108 + 2\tan^{-1}[0.9671396\cdot\tan(0.00860\cdot(J-186))] \quad (6)$$

where D is the daylength ($h^{-1}$), p is the daylength coefficient (°), L is latitude (°), Φ is the Sun's declination angle, J is day of the year and θ is the revolution angle.

This calculation is time accurate to within one minute for latitudes between 40° N/S, increasing to seven minutes up to latitudes between 60° N/S (Forsythe *et al.*, 1995).

*Iron within the mixed layer*

Based on measurements from Rijkenberg *et al.* (2008), Fe(III) speciation in the tropical North Atlantic Ocean produces free iron (Fe′) concentrations below what is required to support *Trichodesmium* growth. In contrast, Fe(II) concentrations are several orders of magnitude greater than Fe(III)′, and are therefore an important source of bioavailable iron for *Trichodesmium*. Previous studies report that Fe(II) accounts for 20% of surface dissolved Fe (dFe) concentrations in the Baltic (Breitbarth *et al.*, 2009), 12-14% in the Pacific (Hansard *et al.*, 2009) and 5-65% in the South Atlantic and Southern Ocean (Bowie *et al.*, 2002, Sarthou *et al.*, 2011). Based on these observations we assumed a global estimate where 25% of dFe is present as Fe(II).

*Growth rate limitation maps*

For each month, at each timescale, the degree to which temperature, irradiance and iron limits *Trichodesmium* IMS101 growth was calculated as follows:

$$\text{SST Limitation} = \frac{\mu_{max}' \left\{ \sin\left[ \pi \left( \frac{T - T_{min}}{T_{max} - T_{min}} \right)^{\theta} \right] \right\}^{\Phi}}{\mu_{max}'} \quad (7)$$

$$\text{E Limitation} = \left\{ 1 - \exp\left( \frac{-E}{E_{k\alpha}} \right) \right\} \cdot \exp\left( -E \cdot E_{k\beta} \right) \quad (8)$$

$$\text{Fe Limitation} = \frac{Fe'}{(K_m + Fe')} \quad (9)$$

where T (°C), E (mol photons $m^{-2}$ $d^{-1}$) and Fe′ (pM) correspond to the spatial resolved oceanographic data values, and $\mu_{max}'$, $T_{min}$, $T_{max}$, $E_{k\alpha}$, $E_{k\beta}$ and $K_m$ are the model parameterisation values as reported in Table S1. All limitation plots exhibit a scale ranging from 0 (no growth potential) to 1 (no limitation to maximal growth) (Fig. S2-S4).

*Global Primary Production*

To estimate *Trichodesmium's* contribution to current ocean production, we applied our growth rate model (Equation 1) to a map of *Trichodesmium* biomass; inferred from a map of *nif*H gene abundance (Tang & Cassar, 2019). The modelled *nif*H gene abundance was converted into *Trichodesmium* biomass (mg C $m^{-2}$) by multiplying by the same assumed 0.3 conversion factor (mg C/$10^6$ *nif*H copies) as reported in Luo *et al.* (2012).

Global growth rates were re-calculated using the same mean monthly oceanographic data used by Tang and Cassar (2019) to generate their map of *nif*H gene abundance, which included sea surface temperature (SST) (°C) from SeaWIFS, PAR in the MLD (mol photons $m^{-2}$ $d^{-1}$) from MODIS and dissolved iron (dFe) (nM) from Community Earth System Model (CESM1-BGC). Note, we used the same global assumption that 25% of dFe is present as Fe(II). Data from the supporting information of Tang and Cassar (2019) was downloaded (https://doi.org/10.1594/PANGAEA.905108) and interpolated to a 1-degree resolution. *Trichodesmium's* mean annual primary production (g C $m^{-2}$ $yr^{-1}$) was calculated as follows:

$$PP = \sum_{1}^{12} B(t) \cdot \mu(t) \cdot N(t) \quad (10)$$

where B(t) is the mean biomass (g C $m^{-2}$) in each of the 12 months, μ(t) is the mean growth rate ($d^{-1}$) and N(t) is the number of days in the month. Annual primary production was converted to annual nitrogen fixation using a C:N ratio of 7.8 (mol:mol) (Boatman *et al.*, 2018b), which corresponds to the present day (mid $CO_2$) condition.

## Results

### *The role of temperature and $pCO_2$ in Trichodesmium biogeography*

*Trichodesmium's* fundamental niche is principally set by its thermal niche width (*w*), which is the range between the minimum ($T_{min}$) and maximum ($T_{max}$) temperature tolerance limits for growth. Our growth rate model estimates $T_{min}$ as 19.50 °C and $T_{max}$ as 30.94 °C, with both parameters being independent of $CO_2$, irradiance and iron concentration (Table S1). Although values for $T_{max}$ as high as 36.5 °C have been reported for this species (Breitbarth *et al.* (2007), data on the *in situ* distribution of *Trichodemsium* are consistent with $T_{max}$ close to 31 °C (Fig. 1).

Modelling *Trichodesmium* growth as a function of SST and $CO_2$ reveals a single equatorial species distribution belt during the LGM, with the niche constrained to lower latitudes during the LGM than at present day (Fig 2). In contrast, *Trichodesmium's* niche will continue to expand into higher latitudes by the end of this century, and will exhibit a niche reduction in certain equatorial regions due to mean SST's exceeding $T_{max}$; this in turn creates a dual equatorial species distribution belt (Fig 2). Overall, the geographical area corresponding to *Trichodesmium's* fundamental niche has increased by ~32% from the LGM to present day, but will decrease by ~9% from present day to the the end of this century (Table 1). This estimate relates to changes in total ocean area only, and does not account for how area of optimal growth conditions will vary.

Our *Trichodesmium* growth model shows that the maximal growth rate that can be achieved under low, mid and high $CO_2$ conditions associated to the LGM, present day and end of this century are 0.204 $d^{-1}$, 0.324 $d^{-1}$ and 0.357 $d^{-1}$, respectively. It also estimates that the optimal temperature for *Trichodesmium* growth ($T_{opt}$) is 25.85°C. At this optimal temperature, and under the low $CO_2$ condition associated with the LGM, regions where SST was sufficient to support a growth rate > 0.15 $d^{-1}$ (a rate equal to 72% of $\mu_{max}$ under these conditions) were 1.7 times lower than at present, but are projected to decrease by 10% from the present day to the end of this century (Table S4). Our results also show that at the optimal temperature and under present day and future $CO_2$ conditions, the area where SST allows *Trichodemsium* to grow at > 0.25 $d^{-1}$ (> 70% and 75% of maximum growth rate under optimal temperature at mid and high $CO_2$ levels) will not significantly change by the end of this century (Table S4).

*The role of temperature, irradiance and $pCO_2$ in Trichodesmium biogeography*

Incorporating the effect of irradiance into calculations based on our SST and $CO_2$ model did not change the spatial distribution of *Trichodesmium* at the LGM, present day and end of this century, but did reduce areas associated with high growth rates (Fig. 3). Our *Trichodesmium* growth model estimates that the optimal irradiance for *Trichodesmium* growth ($E_{opt}$) is 320 μmol photons $m^{-2}$ $s^{-1}$, and is independent of temperature, $CO_2$ and Fe. As such, under the low, mid and high $CO_2$ conditions associated to the LGM, present day and end of this century, maximum *in situ* growth rates were still found to be 0.204 $d^{-1}$, 0.324 $d^{-1}$ and 0.357 $d^{-1}$, respectively. Regions where both SST and irradiance were sufficient to support a growth rate > 0.15 $d^{-1}$ were 1.9 times lower at the

LGM than at present, but are projected to decrease by 10% from the present to the end of this century (Table S5). In contrast, our results also show that under current and projected future $CO_2$ conditions, the area where SST and irradiance allow *Trichodemsium* to grow at > 0.25 $d^{-1}$ (> 70% and 75% of maximum growth rate under optimal temperature at mid and high $CO_2$ levels) is projected to increase by 7% by the end of this century (Table S5).

*The role of temperature, irradiance, iron and $pCO_2$ in Trichodesmium biogeography*

Incorporating the effect of iron into calculations based on our SST, irradiance and $CO_2$ model did not change the spatial distribution of *Trichodesmium* at the LGM, present day and end of this century, but did cause an even greater reduction of areas associated with high growth rates (Fig. 4). Our model estimates that the half saturation concentration of iron for *Trichodesmium* growth ($K_m$) is constant at 185.5 pM, and is independent of $CO_2$, and irradiance at a temperature of 26 °C. We did not assess the interaction of Fe-limitation with temperature in our experiments, a point that we discuss below. Modelling growth rates onto maps of SST, irradiance and iron, showed that the highest achieved *in situ* growth rates were lower than the maximum Fe-replete rates (i.e. 0.172 $d^{-1}$ versus 0.204 $d^{-1}$ at low $CO_2$, 0.269 $d^{-1}$ versus 0.342 $d^{-1}$ at present $CO_2$ and 0.305 $d^{-1}$ versus 0.357 $d^{-1}$ at high $CO_2$ conditions). Regions where SST, irradiance and iron were sufficient to support a growth rate > 0.15 $d^{-1}$ were almost an order of magnitude lower at the LGM than at present, but are not projected to change substantially (decrease of 1%) by the end of this century (Table S6). Our results also show that under present and projected future $CO_2$ conditions, the area where SST, irradiance and Fe are sufficient to allow *Trichodemsium* to grow at > 0.25 $d^{-1}$ is projected to increase by 173% by the end of this century (Table S6).

*Temperature-dependence of iron saturation*

Our *Trichodesmium* growth model (Eq. 1) assumes a multiplicative interaction of the effects of temperature, $CO_2$, irradiance and Fe on growth rate. The experimental data used for parameter estimation included three $CO_2$ levels at both a light-saturating and light-limiting irradiance at 21 temperatures in the range 19 to 32 °C giving us high confidence that a multiplicative interaction of these variables is correct. However, the effect of Fe limitation on growth was only determined at

the optimum temperature for growth of 26 °C. Although our data at this temperature indicates a multiplicative interaction of the effects of $CO_2$, irradiance and Fe on growth rate, we did not measure the Fe dependence of growth at other temperatures.

In our model we assume that *Trichodesmium's* $K_m$ for Fe-limited growth is independent of temperature, which is consistent to the observation that the relationship between the relative degree of iron limitation of growth rate and the concentration of biologically available dissolved Fe varied little with temperature in the diatom *Thalassiosira pseudoana* (Sunda & Huntsman, 2011). In contrast to this assumption, Jiang *et al.* (2018) reported that *Trichodesmium* exhibits a temperature dependency of $K_m$; with values decreasing by up to 84% from the value at the optimal growth temperature at sub- and supra-optimal temperatures. Jiang *et al.* (2018) concluded that this temperature dependence of $K_m$ could result in a large increase in growth and $N_2$ fixation under the SST projected for the end of this century, with the global marine $N_2$ fixation rates increasing by ~22%.

We assessed the effect that using a temperature-dependence of $K_m$ similar to that reported by Jiang *et al.* (2018) (Fig. S8) has in our growth rate model. When we did this, ocean area with optimal SST, optimal irradiance and iron ($\mu > 0.15$ $d^{-1}$) were 8% lower in the present and 37% greater in the future when a temperature dependent $K_m$ instead of a constant $K_m$ (see Table 1). Furthermore, regions where SST, irradiance and iron were sufficient to support a growth rate > 0.25 $d^{-1}$ were 90% lower in the present and 29% greater in the future when a temperature dependant $K_m$ was used instead of a constant $K_m$ (see Table 1). Thus, regions where *Trichodemisum* can achieve high growth rates are projected to increase in area by 787% from the present to the end of this century when a temperature dependant $K_m$ is used (Table S7), much greater than the 173% increase that we calculated using a constant temperature invariant $K_m$ (Table S6).

**Discussion**

Our model of the dependence of *Trichodesmium* growth rates on four key abiotic variables (temperature, irradiance, $pCO_2$ and iron) (Fig. 1a-e) was based on previous experiments (Boatman *et al.*, 2017, Boatman *et al.*, 2018c), where the difference in growth rate between experiments at identical growth conditions was < 5%. The growth rate data was obtained for cultures that were in

balanced growth. Other studies report somewhat different thermal tolerance limits (Boyd *et al.*, 2013, Breitbarth *et al.*, 2007), and $CO_2$ dependencies of growth rate (Eichner *et al.*, 2014, Shi *et al.*, 2012); however, these were obtained from experiments with lower data resolution at the temperature limits for growth, and short culture acclimation times. Overall, we have confidence in our previous studies and Equation 1, which is based on those previous results.

*A representative model for the Trichodesmium genus*

A notable consideration of our *Trichodesmium* growth model (Equation 1) is that it is based on data for *Trichodesmium erythraeum*, but the *Trichodesmium* genus includes six species assigned to four clades (Lundgren *et al.*, 2005): although the lower and upper temperature limits that we measured for *T. erythraaeum* IMS101 are nearly identical to the temperature limits currently observed for *Trichodesmium* spp. in nature from shipboard samples (Fig. 1f). Recent studies indicate that other species including *T. thiebuatii* (Rouco *et al.*, 2014) and *T. tenue* (Chappell & Webb, 2010) are more abundant in nature than *T. erythraeum*. Unfortunately, these other species have not been subjected to the same rigorous laboratory investigations of their growth requirements. In addition, our model does not account for the potential evolution of *Trichodesmium* to elevated temperature and/or $CO_2$ as the ocean warms. For example, previous research has indicated that prolonged (~ 6.5 years) exposure to future elevated $CO_2$ concentrations causes *Trichodesmium* to significantly, and irreversibly increase $N_2$ fixation and growth rates (Hutchins *et al.*, 2015).

*Trichodesmium's fundamental niche under nutrient saturation*

Based on SST alone, Breitbarth *et al.* (2007) projected an 11% increase in the spatial distribution of *Trichodesmium* by the end of this century, but with a 16% decrease in areas they defined as optimal for growth. Our results do not support these findings, instead showing a 9% decrease in the spatial distribution by the end of this century, with no significant difference (-0.2%) in areas with optimal SST for growth. The causes of these contradictory findings are i), a difference in the predicted global maps of oceanographic SST ii), a difference in *Trichodesmium's* maximum temperature limit for growth ($T_{max}$), which we define as 31 °C and Breitbarth *et al.* (2007) defined

as 36.5 °C and iii), a difference in the definition of optimal condition, where Breitbarth *et al.* (2007) used a thermal range (24 – 30 °C) while we opted to use a growth rate threshold ($\mu > 0.25$ $d^{-1}$).

Incorporating irradiance into our SST and $CO_2$ model led to a projected 7% increase in areas defined as optimal for growth from the present to the end of this century. This increase is due to a projected increase in water stratification and a shallower mixed layer (Fig. S9). This in turn reduces the supply of nitrate from deep water into the surface waters, which in turn leads to lower phytoplankton biomass, as indicated by the modelled reduction in surface chlorophyll *a* (Fig. S10) and dissolved organic carbon concentrations (Fig. S11). The decrease in biomass causes a decrease in light attenuation (Fig. S12), resulting in higher mean irradiances within the mixed layer, and a 7% increase in *Trichodesmum*'s growth potential.

*The role of nutrient-limitation in Trichodesmium biogeography*

Although temperature and irradiance are the principal factors that determine the potential geographical range of *Trichodesmium*, iron is a major factor that determines growth rates. This is because *Trichodesmium* has a high cellular requirement for iron due to an extensive suite of metalloenzymes, including nitrogenase, proteins in the photosynthetic reaction centres and ferredoxin (Kustka *et al.*, 2003), and to the low solubility and short residence time of Fe in seawater (Liu & Millero, 2002). Low iron concentrations limit *Trichodesmium's* productivity and growth in many ocean regions (Berman-Frank *et al.*, 2001, Berman-Frank *et al.*, 2007). Including iron limitation into our model substantially reduced estimates of global growth rates (Table S6). In addition, many regions within the geographic range that are close to the optimal temperature for nutrient-replete growth, exhibited low or no growth when iron was included into the model (Fig. 4). Regions where growth remained relatively high included waters off the west coasts of Africa and Australia; most likely due to the contribution of dust deposition of iron into the surface waters. Aeolian dust has been shown to benefit *Trichodesmium* by providing a source of bioavailable iron (Basu *et al.*, 2019, Basu & Shaked, 2018).

We applied the same constants for the half saturation concentration for Fe and fraction of bioavailable dFe across all seasons and timescales (i.e. LGM, Present, Future). Thus, changes in

growth potential over time, notably the 173% increase in the area associated to > 0.25$d^{-1}$ by the end of this century, are solely driven by changes in the dissolved iron concentration (dFe) (Fig. S13). The IPSL-CM5A-LR earth system model uses PISCES (Pelagic Interaction Scheme for Carbon and Ecosystem Studies) (Aumont & Bopp, 2006) to simulate all major nutrients including iron. In terms of inputs, atmospheric deposition is estimated from INCA (Integrated Nitrogen Catchment model) (Aumont *et al.*, 2008); river discharge of carbon and nutrients is taken from Ludwig *et al.* (1996); and iron input from sediment mobilisation as parameterised in Aumont and Bopp (2006). These sources are explicitly included but do not vary in time apart from a climatological seasonal cycle for the atmospheric input. Thus, the increase in dFe modelled from present day to the end of the century is not due to iron inputs, rather the relationship between pools. For example, a higher dFe could be due to less complexed iron, reduced demand by phytoplankton growth, increased zooplankton exudation or reduced loss of particulate iron from sinking sediment whether by higher remineralisation, reduced scavenging/aggregation or lower bacterial uptake.

It is worth noting that the relationship between dFe and complexed iron within PISCES uses a basic description of iron-ligand interactions, and does not account for how future conditions (i.e. ocean acidification) will alter the organic chelation of iron. We acknowledge that this is a shortcoming in our projections of the future growth potential of *Trichodesmium* given the importance of dFe data to our iron-integrated modelling outcomes; and highlight this is an area requiring further work in order to improve projections of future ocean trace metal chemistry. We did not consider the potential role of phosphorus-limitation in our model. Diazotrophs are reported to be iron limited in the Pacific and Indian Ocean, and phosphorus limited (Misumi *et al.*, 2014) or phosphorus-iron co-stressed (Held *et al.*, 2020, Mills *et al.*, 2004) in the Atlantic Ocean. A reduction in dust deposition could have major implications for the phosphorus pool as well as iron. Whilst phosphorus (P) was not integrated into our growth rate model, *Trichodesmium* may be able to alleviate P-limitation by utilising organic sources of phosphorus (Dyhrman *et al.*, 2006, Sohm & Capone, 2006). Alternatively, *Trichodesmium* colonies larger than 1 mm may alleviate P-limitation by vertically migrating below the phosphocline to assimilate phosphate and rising back to the surface of the euphotic zone (White *et al.*, 2006). A recent study by Garcia *et al.* (2015) showed that under P-deficiency, *Trichodesmium* cells grew and fixed nitrogen faster with concurrent iron-limitation than when iron was replete. This could have significant implications for

*Trichodesmium's* growth potential, particularly in the Atlantic Ocean, with more emphasis on SST and irradiance in determining the fundamental niche.

*Trichodesmium production*

Calculating *Trichodesmium*'s global primary production requires information on the oceanographic distributions of both biomass and growth rate. Recently, a data driven map of the global *Trichodesmium nif*H abundance was provided by Tang and Cassar (2019). In this paper, a large but still geographically limited database of *Trichodesmium nif*H gene abundance was extrapolated to the global ocean. Here we estimate *Trichodesmium*'s contribution to present day ocean production by converting Tang and Cassar (2019) modelled *nif*H abundance to carbon biomass, and then multiplying by our map of mean growth rate (Fig. 5).

We estimate that *Trichodesmium* fixes 0.347 Pg C $yr^{-1}$, which represents a contribution of 0.58-0.96% of the total ocean primary production of 36-60 Pg C $yr^{-1}$ (Carr *et al.*, 2006). Assuming a C:N ratio of 7.8 (mol:mol) under present day conditions (Boatman *et al.*, 2018b), we calculate *Trichodesmium's* annual mean N productivity to be 51.8 Tg N $yr^{-1}$. Based on global ocean estimates of $N_2$ fixation being 62 (52-73) Tg N $yr^{-1}$ (Luo *et al.*, 2012), *Trichodesmium* would account for 84% of global diazotrophy. These estimates were made using a constant $K_m$ value for iron-limited growth; however, using a temperature-dependent $K_m$ value increases primary production to 0.380 Pg C $yr^{-1}$ and $N_2$ fixation to 56.8 Tg N $yr^{-1}$, which represents 0.64-1.05% and 91.6% of the total annual mean C and N productivity, respectively (Table S8).

Although such an approach was employed for the present data, we did not apply it to the LGM, or to project into the future as the current relationship between *Trichodesmium* abundance and oceanographic variables will most likely breakdown for other climate regimes. This is because the prevailing climate regime will affect not only ocean circulation but also competition of *Trichodesmium* with other phytoplankton, including other diazotrophs, as well as trophic interactions with grazers and pathogens. It's also worth noting that the growth rates used in these productivity calculations were dependent on temperature, light and iron only, and do not include rate limiting factors such as competition and trophic interactions. As such, these estimates should be considered as the upper limit for *Trichodesmium's* relative contribution to the C and N cycle.

## Conclusion

Our analysis indicates that the increase of SST from the LGM to present has allowed *Trichodesmium's* range to expand to higher latitudes. Future increases of SST from the present to the end of this century are projected to cause a range expansion at high latitudes and a range contraction in the tropics (Fig. 2). The former is driven by the poleward shift of the 20 °C isotherm, whilst the latter will be due to the SST exceeding the maximum thermal tolerance limit for growth (31 °C). We also found that although the increase of $pCO_2$ from the LGM to the present has allowed growth rates to nearly double under nutrient-replete conditions (Fig. 2), future increases of $CO_2$ will have little direct effect on the growth rate of *Trichodesmium*.

Increased water stratification and a shallower mixed layer in the future ocean will limit the supply of nitrate to the surface waters. Since these stratified waters are already N-limited, this should benefit *Trichodesmium* and other diazotrophs, as competition with N-limited phytoplankton for Fe and P may decrease. It is also likely that the surface Chl *a* concentration will decline as more of the ocean becomes increasingly N-limited (Zehr & Kudela, 2011); this should in turn decrease light attenuation leading to a higher mean irradiance within the shallower mixed layer. Higher irradiance will increase the rate of iron photoreduction. This coupled to the increase in Fe(II) caused by ligand dissociation under more acidified conditions (Shi *et al.*, 2010) should increase the bioavailablity of Fe to *Trichodesmium*.

Such future changes could significantly increase *Trichodesmium's* global productivity (Hutchins *et al.*, 2007), which given the relative contribution to global annual mean N production, suggests a potentially significant negative feedback to the increasing atmospheric $CO_2$ concentrations that have been and continue to be caused by fossil fuel burning and deforestation.

## Acknowledgements

This research was supported by a UK Natural Environment Research Council PhD studentship (NE/J500379/1) to TGB and NERC grant (NE/P002374/1) to RJG. The authors thank Erik Buitenhuis from the School of Environmental Sciences, University of East Anglia, for helping

extract oceanographic data sets and Martha Gledhill from GEOMAR, Helmholtz Centre for Ocean Research, for advice and knowledge on trace metal chemistry. The authors declare that the research was conducted in the absence of any commercial or financial relationships that could be construed as a potential conflict of interest.

## Author Contributions

TGB and RJG conceived the study and developed the modelling approach. TGB, RJG and TL designed the initial growth rate laboratory experiments that the model was based on. All laboratory experiments were conducted by TGB, who also processed the primary data. TGB and GJCU performed model parameter optimisation. TGB handled all oceanographic data and processed the global data files. The fundamental niche data were processed by TGB and jointly analysed by TGB, TL and RJG. All figures and tables were generated by TGB. The initial draft of the main text was made by TGB. Iterations of the manuscript were implemented by TGB, GJGU, TL and RJG. The submitted version of the manuscript is approved for publication by TGB, GJGU, TL and RJG.

## Data Sharing and Data Accessibility

The data that supports the findings of this study are available in the supplementary material of this article.

## References

Arrigo KR (2007) Carbon cycle: marine manipulations. Nature, **450**, 491.

Aumont O, Bopp L (2006) Globalizing results from ocean *in situ* iron fertilization studies. Global biogeochemical cycles, **20**, GB2017.

Aumont O, Bopp L, Schulz M (2008) What does temporal variability in aeolian dust deposition contribute to sea‐surface iron and chlorophyll distributions? Geophysical Research Letters, **35**.

Barcelos E Ramos J, Biswas H, Schulz KG, Laroche J, Riebesell U (2007) Effect of rising atmospheric carbon dioxide on the marine nitrogen fixer *Trichodesmium*. Global biogeochemical cycles, **21**, GB2028.

Basu S, Gledhill M, De Beer D, Matondkar SP, Shaked Y (2019) Colonies of marine cyanobacteria *Trichodesmium* interact with associated bacteria to acquire iron from dust. Communications biology, **2**, 1-8.

Basu S, Shaked Y (2018) Mineral iron utilization by natural and cultured *Trichodesmium* and associated bacteria. Limnology and Oceanography, **63**, 2307-2320.

Berman-Frank I, Cullen JT, Shaked Y, Sherrell RMF, P.G. (2001) Iron availability, cellular iron quotas, and nitrogen fixation in *Trichodesmium*. Limnology and Oceanography, **46**, 1249-1260.

Berman-Frank I, Quigg A, Finkel ZV, Irwin AJ, Haramaty L (2007) Nitrogen-fixation strategies and Fe requirements in cyanobacteria. Limnology and Oceanography, **52**, 2260-2269.

Boatman TG, Davey PA, Lawson T, Geider RJ (2018a) $CO_2$ modulation of the rates of photosynthesis and light-dependent $O_2$ consumption in *Trichodesmium*. Journal of Experimental Botany, ery368.

Boatman TG, Lawson T, Geider RJ (2017) A Key Marine Diazotroph in a Changing Ocean: The Interacting Effects of Temperature, $CO_2$ and Light on the Growth of *Trichodesmium erythraeum* IMS101. PLoS One, **12**, e0168796.

Boatman TG, Mangan NM, Lawson T, Geider RJ (2018b) Inorganic carbon and pH dependency of photosynthetic rates in *Trichodesmium*. Journal of Experimental Botany, ery141.

Boatman TG, Oxborough K, Gledhill M, Lawson T, Geider R (2018c) An integrated response of *Trichodesmium erythraeum* IMS101 growth and photo-physiology to iron, $CO_2$ and light intensity. Frontiers in microbiology, **9**, 624.

Bowie AR, Achterberg EP, Sedwick PN, Ussher S, Worsfold PJ (2002) Real-time monitoring of picomolar concentrations of iron (II) in marine waters using automated flow injection-chemiluminescence instrumentation. Environmental science & technology, **36**, 4600-4607.

Boyd PW, Rynearson TA, Armstrong EA *et al.* (2013) Marine phytoplankton temperature versus growth responses from polar to tropical waters–outcome of a scientific community-wide study. PLoS One, **8**, e63091.

Breitbarth E, Gelting J, Walve J, Hoffmann LJ, Turner D, Hassellöv M, Ingri J (2009) Dissolved iron (II) in the Baltic Sea surface water and implications for cyanobacterial bloom development. Biogeosciences (BG), **6**, 2397-2420.

Breitbarth E, Oschlies A, Laroche J (2007) Physiological constraints on the global distribution of *Trichodesmium* - effect of temperature on diazotrophy. Biogeosciences, **4**, 53-61.

Buesseler KO, Boyd PW (2009) Shedding light on processes that control particle export and flux attenuation in the twilight zone of the open ocean. Limnology and Oceanography, **54**, 1210-1232.

Cai X, Gao K (2015) Levels of daily light doses under changed day-night cycles regulate temporal segregation of photosynthesis and $N_2$ fixation in the Cyanobacterium *Trichodesmium erythraeum* IMS101. PLoS One, **10**, e0135401.

Capone DG (2005) Nitrogen fixation by *Trichodesmium* spp.: An important source of new nitrogen to the tropical and subtropical North Atlantic Ocean. Global biogeochemical cycles, **19**.

Carr M-E, Friedrichs MA, Schmeltz M *et al.* (2006) A comparison of global estimates of marine primary production from ocean color. Deep Sea Research Part II: Topical Studies in Oceanography, **53**, 741-770.

Chappell PD, Webb EA (2010) A molecular assessment of the iron stress response in the two phylogenetic clades of *Trichodesmium*. Environmental Microbiology, **12**, 13-27.

Dennison WC, Orth RJ, Moore KA *et al.* (1993) Assessing water quality with submersed aquatic vegetation. BioScience, **43**, 86-94.

Doney SC, Yeager S, Danabasoglu G, Large WG, Mcwilliams JC (2007) Mechanisms governing interannual variability of upper-ocean temperature in a global ocean hindcast simulation. Journal of Physical Oceanography, **37**, 1918-1938.

Duce R, Laroche J, Altieri K *et al.* (2008) Impacts of atmospheric anthropogenic nitrogen on the open ocean. Science, **320**, 893-897.

Dufresne J-L, Foujols M-A, Denvil S *et al.* (2013) Climate change projections using the IPSL-CM5 Earth System Model: from CMIP3 to CMIP5. Climate Dynamics, **40**, 2123-2165.

Dyhrman ST, Chappell PD, Haley ST, Moffett JW, Orchard ED, Waterbury JB, Webb EA (2006) Phosphonate utilization by the globally important marine diazotroph *Trichodesmium*. Nature, **439**, 68-71.

Eichner M, Kranz SA, Rost B (2014) Combined effects of different $CO_2$ levels and N sources on the diazotrophic cyanobacterium *Trichodesmium*. Physiologia Plantarum, **152**, 316-330.

Falkowski PG, Raven JA (1997) *Aquatic photosynthesis*, Blackwell Science Malden, MA.

Field CB, Behrenfeld MJ, Randerson JT, Falkowski P (1998) Primary production of the biosphere: integrating terrestrial and oceanic components. Science, **281**, 237-240.

Forsythe WC, Rykiel Jr EJ, Stahl RS, Wu H-I, Schoolfield RM (1995) A model comparison for daylength as a function of latitude and day of year. Ecological Modelling, **80**, 87-95.

Garcia NS, Fu F, Sedwick PN, Hutchins DA (2015) Iron deficiency increases growth and nitrogen-fixation rates of phosphorus-deficient marine cyanobacteria. ISME Journal, **9**, 238-245.

Hansard SP, Landing WM, Measures CI, Voelker BM (2009) Dissolved iron (II) in the Pacific Ocean: measurements from the PO2 and P16N CLIVAR/$CO_2$ repeat hydrography expeditions. Deep Sea Research Part I: Oceanographic Research Papers, **56**, 1117-1129.

Helbling EW, Villafañe V, Holm-Hansen O (1994) *Effects of ultraviolet radiation on Antarctic marine phytoplankton photosynthesis with particular attention to the influence of mixing*, Wiley Online Library.

Held NA, Webb EA, Mcilvin MM *et al.* (2020) Co-occurrence of Fe and P stress in natural populations of the marine diazotroph *Trichodesmium*. Biogeosciences, **17**, 2537-2551.

Ho T-Y, Chu T-H, Hu C-L (2013) Interrelated influence of light and Ni on *Trichodesmium* growth. Frontiers in microbiology, **4**, 1-6.

Hutchins D, Fu FX, Zhang Y *et al.* (2007) $CO_2$ control of *Trichodesmium* $N_2$ fixation, photosynthesis, growth rates, and elemental ratios: implications for past, present, and future ocean biogeochemistry. Limnology and Oceanography, **52**, 1293-1304.

Hutchins DA, Walworth NG, Webb EA *et al.* (2015) Irreversibly increased nitrogen fixation in *Trichodesmium* experimentally adapted to elevated carbon dioxide. Nature communications, **6**, 8155.

Jiang H-B, Fu F-X, Rivero-Calle S *et al.* (2018) Ocean warming alleviates iron limitation of marine nitrogen fixation. Nature Climate Change, **8**, 709.

Kohfeld KE, Ridgwell A (2009) Glacial-interglacial variability in atmospheric $CO_2$. Surface ocean-lower atmosphere processes, **187**, 251-286.

Kustka AB, Sanudo-Wilhelmy SA, Carpenter EJ, Capone D, Burns J, Sunda WG (2003) Iron requirements for dinitrogen-and ammonium-supported growth in cultures of *Trichodesmium* (IMS 101): Comparison with nitrogen fixation rates and iron: carbon ratios of field populations. Limnology and Oceanography, **48**, 1869-1884.

Langhans RW, Tibbitts T (1997) Plant growth chamber handbook.

Levitan O, Rosenberg G, Setlik I *et al.* (2007) Elevated $CO_2$ enhances nitrogen fixation and growth in the marine cyanobacterium *Trichodesmium*. Global Change Biology, **13**, 531-538.

Liu X, Millero FJ (2002) The solubility of iron in seawater. Marine Chemistry, **77**, 43-54.

Low‐Décarie E, Boatman TG, Bennett N, Passfield W, Gavalás‐Olea A, Siegel P, Geider RJ (2017) Predictions of response to temperature are contingent on model choice and data quality. Ecology and Evolution, **7**, 10467-10481.

Ludwig W, Amiotte Suchet P, Probst J-L (1996) River discharges of carbon to the world's oceans: determining local inputs of alkalinity and of dissolved and particulate organic carbon. Sciences de la terre et des planètes (Comptes rendus de l'Académie des sciences), **323**, 1007-1014.

Lundgren P, Janson S, Jonasson S, Singer A, Bergman B (2005) Unveiling of novel radiations within *Trichodesmium* cluster by hetR gene sequence analysis. Applied and environmental microbiology, **71**, 190-196.

Luo Y, Doney S, Anderson L *et al.* (2012) Database of diazotrophs in global ocean: abundance, biomass and nitrogen fixation rates. pp Page, Earth System Science Data.

Mahowald NM, Luo C (2003) A less dusty future? Geophysical Research Letters, **30**.

Michaelis L, Menten ML (1913) Die kinetik der invertinwirkung. Biochem. z, **49**, 352.

Millero FNJ (2009) Effect of ocean acidification on the speciation of metals in seawater. Oceanography, **22**, 72-85.

Mills MM, Ridame C, Davey M, La Roche J, Geider RJ (2004) Iron and phosphorus co-limit nitrogen fixation in the eastern tropical North Atlantic. Nature, **429**, 292-294.

Misumi K, Lindsay K, Moore JK, Doney SC, Bryan FO, Tsumune D, Yoshida Y (2014) The iron budget in ocean surface waters in the 20th and 21st centuries: projections by the Community Earth System Model version. Biogeosciences, **11**.

Monteiro FM, Dutkiewicz S, Follows MJ (2011) Biogeographical controls on the marine nitrogen fixers. Global biogeochemical cycles, **25**, 1-8.

Moore CM, Mills MM, Milne A *et al.* (2006) Iron limits primary productivity during spring bloom development in the central North Atlantic. Global Change Biology, **12**, 626-634.

Platt T, Gallegos CL (1980) Modelling primary production. In: *Primary productivity in the sea.* pp Page., Springer.

Rijkenberg MJ, Powell CF, Dall'osto M *et al.* (2008) Changes in iron speciation following a Saharan dust event in the tropical North Atlantic Ocean. Marine Chemistry, **110**, 56-67.

Rost B, Zondervan I, Wolf-Gladrow D (2008) Sensitivity of phytoplankton to future changes in ocean carbonate chemistry: current knowledge, contradictions and research directions. Marine Ecology Progress Series, **227**, 227-237.

Rouco M, Warren HJ, Mcgillicuddy DJ, Waterbury JB, Dyhrman ST (2014) *Trichodesmium* sp. clade distributions in the western North Atlantic Ocean. Limnology and Oceanography, **59**, 1899-1909.

Sarthou G, Bucciarelli E, Chever F *et al.* (2011) Labile Fe (II) concentrations in the Atlantic sector of the Southern Ocean along a transect from the subtropical domain to the Weddell Sea Gyre. Biogeosciences.

Shi D, Kranz SA, Kim JM, Morel FMM (2012) Ocean acidification slows nitrogen fixation and growth in the dominant diazotroph *Trichodesmium* under low-iron conditions. Proceedings of the National Academy of Sciences, **109**, 3094-3100.

Shi D, Xu Y, Hopkinson BM, Morel FMM (2010) Effect of ocean acidification on iron availability to marine phytoplankton. Science, **327**, 676-679.

Shi T, Sun Y, Falkowski PG (2007) Effects of iron limitation on the expression of metabolic genes in the marine cyanobacterium *Trichodesmium erythraeum* IMS101. Environmental Microbiology, **9**, 2945-2956.

Sohm JA, Capone DG (2006) Phosphorus dynamics of the tropical and subtropical north Atlantic: *Trichodesmium* spp. versus bulk plankton. Marine Ecology Progress Series, **317**, 21.

Spungin D, Berman-Frank I, Levitan O (2014) *Trichodesmium's* strategies to alleviate phosphorus limitation in the future acidified oceans. Environmental Microbiology, **16**, 1935-1947.

Sunda WG, Huntsman SA (2011) Interactive effects of light and temperature on iron limitation in a marine diatom: Implications for marine productivity and carbon cycling. Limnology and Oceanography, **56**, 1475-1488.

Tang W, Cassar N (2019) Data - Driven Modeling of the Distribution of Diazotrophs in the Global Ocean. Geophysical Research Letters, **46**, 12258-12269.

Tegen I, Werner M, Harrison S, Kohfeld K (2004) Relative importance of climate and land use in determining present and future global soil dust emission. Geophysical Research Letters, **31**.

White AE, Spitz YH, Karl DM, Letelier RM (2006) Flexible elemental stoichiometry in Trichodesmium spp. and its ecological implications. Limnology and Oceanography, **51**, 1777-1790.

Zehr JP, Kudela RM (2011) Nitrogen cycle of the open ocean: from genes to ecosystems. Annual Review of Marine Science, **3**, 197-225.

**Table 1.** The geographical areas (M km$^2$) of *Trichodesmium's* fundamental niche ($\mu > 0$ d$^{-1}$) and regions of optimal growth conditions ($\mu > 0.25$ d$^{-1}$) at the last glacial maximum (LGM), the present and projected for the future (est. 2100). Ocean area associated to growth rates ($\mu > 0.25$ d$^{-1}$), were calculated as a function of i), sea surface temperature assuming both irradiance and Fe are not limiting ii), sea surface temperature and irradiance assuming Fe is not limiting and iii), sea surface temperature, irradiance and iron concentration. Note, the maximum growth rate at the LGM was 0.204 d$^{-1}$; therefore, the geographical areas were always zero. The projected ocean area for each month, calculated at varying growth rate thresholds can be found in the supporting information (Table S3-S6). Values in parenthesis are calculated using a temperature dependent $K_m$ (Table S7).

| Ocean area (M km$^2$) | Timescale | Month | |
|---|---|---|---|
| | | February | August |
| Fundamental niche | LGM | 153.8 | 144.5 |
| | Present | 200.6 | 201.7 |

| | | | |
|---|---|---|---|
| | Future | 191.3 | 179.2 |
| | LGM | 0.0 | 0.0 |
| Optimal SST | Present | 123.4 | 116.5 |
| | Future | 128.1 | 116.4 |
| | LGM | 0.0 | 0.0 |
| Optimal SST and E | Present | 94.0 | 69.4 |
| | Future | 98.6 | 77.7 |
| | LGM | 0.0 (0.0) | 0.0 (0.0) |
| Optimal SST, E and Fe | Present | 0.0 (0.1) | 0.1 (0.1) |
| | Future | 0.2 (0.2) | 0.2 (0.3) |

**Figure 1.** The response of *Trichodesmium erythraeum* IMS101 growth rates to iron concentration (a, d), temperature (b, e) and irradiance (c). Growth rates ($d^{-1}$) were calculated as a multiplicative function of temperature, iron and irradiance using Equation 1. Note, temperature and iron responses were measured at low (LL = 40 µmol photons $m^{-2}$ $s^{-1}$) and high (HL = 400 µmol photons $m^{-2}$ $s^{-1}$) light. Shipboard observations of *Trichodesmium* biomass (Luo *et al.*, 2012) are plotted against the sea surface temperature (f); where the dashed lines represent the minimum ($T_{min}$) and maximum ($T_{max}$) temperature limits for growth, and the red line is the temperature-growth response curve under present conditions modelled using Equation (1) with the parameter values reported in the supporting information (Table S1).

**Figure 2.** The distribution of *Trichodesmium erythraeum* IMS101 growth rate ($d^{-1}$) calculated for the mixed layer as a function of sea surface temperature and $CO_2$, assuming optimal irradiance and iron-replete conditions. Maps were generated for February (a, b, c) and August (d, e, f) during the last glacial maximum (LGM) (a, d), for the present (b, e) and projected for the future (est. 2100)

(c, f). Note, a delta growth rate map for (Present-LGM) and (Future-Present) is presented in the supporting information (Fig. S5).

**Figure 3.** The distribution of *Trichodesmium erythraeum* IMS101 growth rate ($d^{-1}$) calculated for the mixed layer as a function of sea surface temperature, $CO_2$ and irradiance, assuming iron-replete conditions. Maps were generated for February (a, b, c) and August (d, e, f) during the last glacial maximum (LGM) (a, d), for the present (b, e) and projected for the future (est. 2100) (c, f). Note, a delta growth rate map for (Present-LGM) and (Future-Present) is presented in the supporting information (Fig. S6).

**Figure 4.** The distribution of *Trichodesmium erythraeum* IMS101 growth rate ($d^{-1}$) calculated for the mixed layer as a function of sea surface temperature, $CO_2$, irradiance and iron concentration. Maps were generated for February (a, b, c) and August (d, e, f) during the last glacial maximum (LGM) (a, d), in the present (b, e) and projected for the future (est. 2100) (c, f). Note, a delta growth rate map for (Present-LGM) and (Future-Present) is presented in the supporting information (Fig. S7).

**Figure 5.** The annual mean growth rate ($d^{-1}$) (a), modelled *nif*H gene abundance ($\log_{10}$ copies $m^{-2}$) (b), biomass (mg C $m^{-2}$) (c) and primary production (g C $m^{-2}$ $yr^{-1}$) (d) of *Trichodesmium erythraeum* IMS101. Growth rates and biomass values were averages across all months and were multiplied to generate the map of primary productivity. Note, global monthly mean primary production values are reported in the supporting information (Table S8).

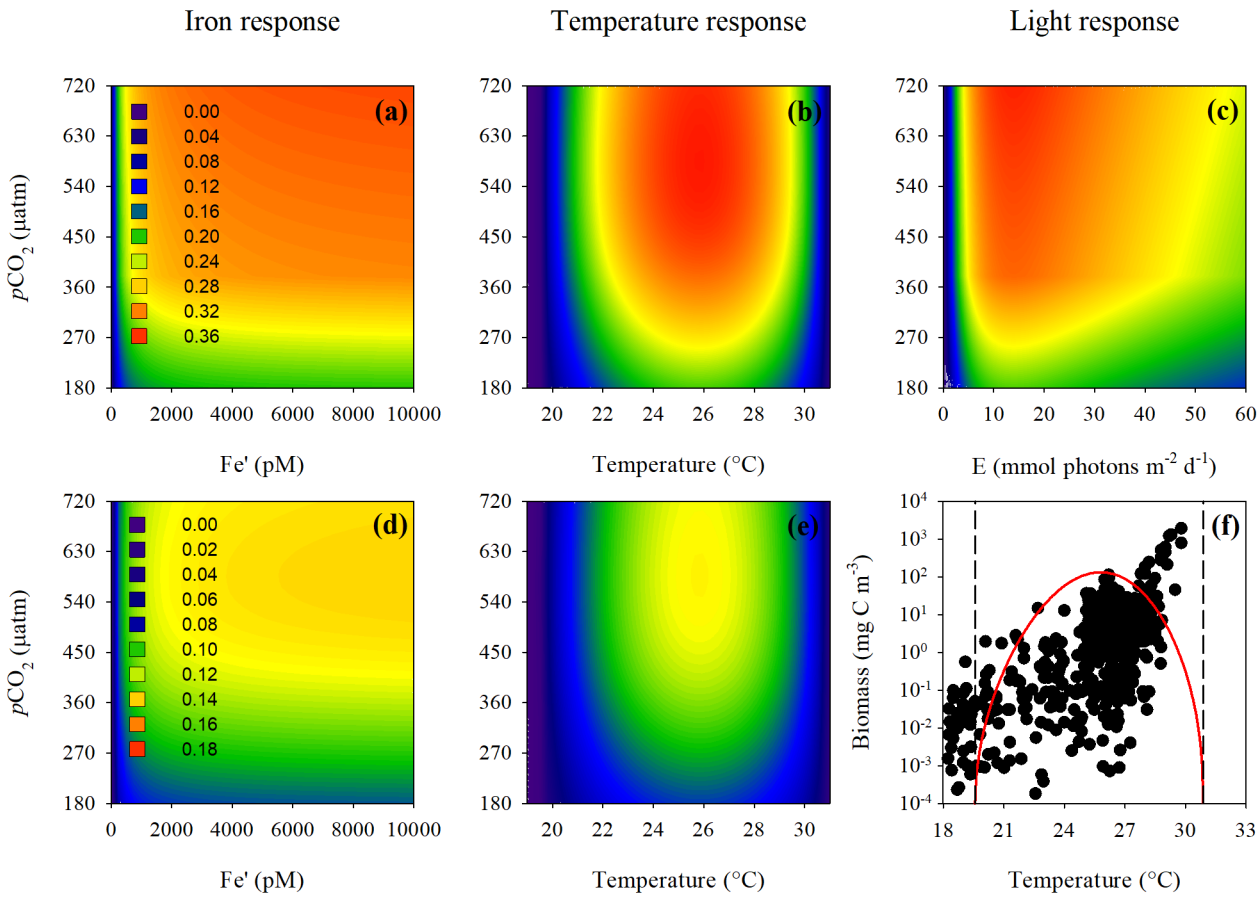


gcb_15324_f1.tif

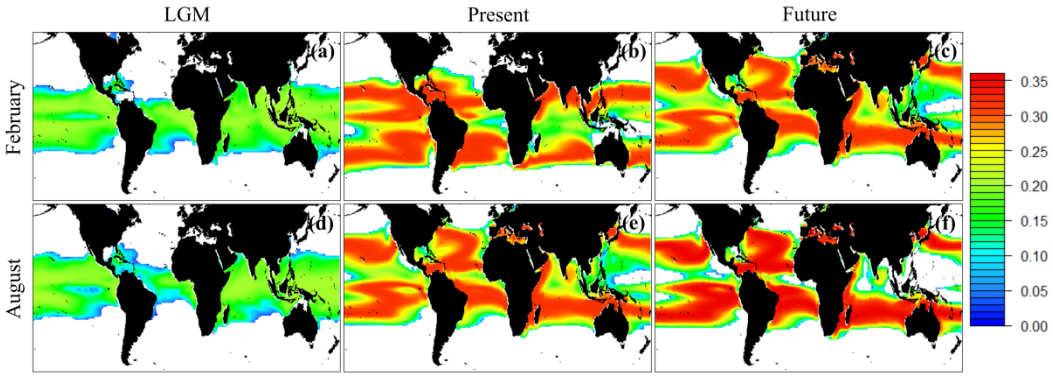


gcb_15324_f2.png

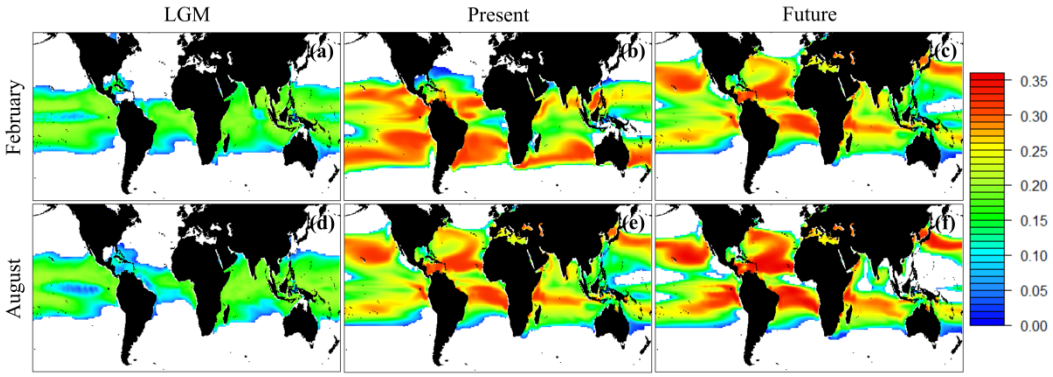


gcb_15324_f3.png

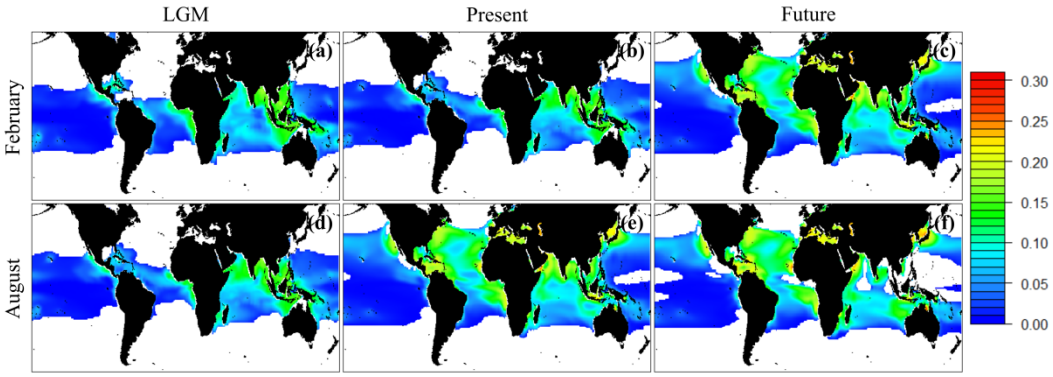


gcb_15324_f4.png

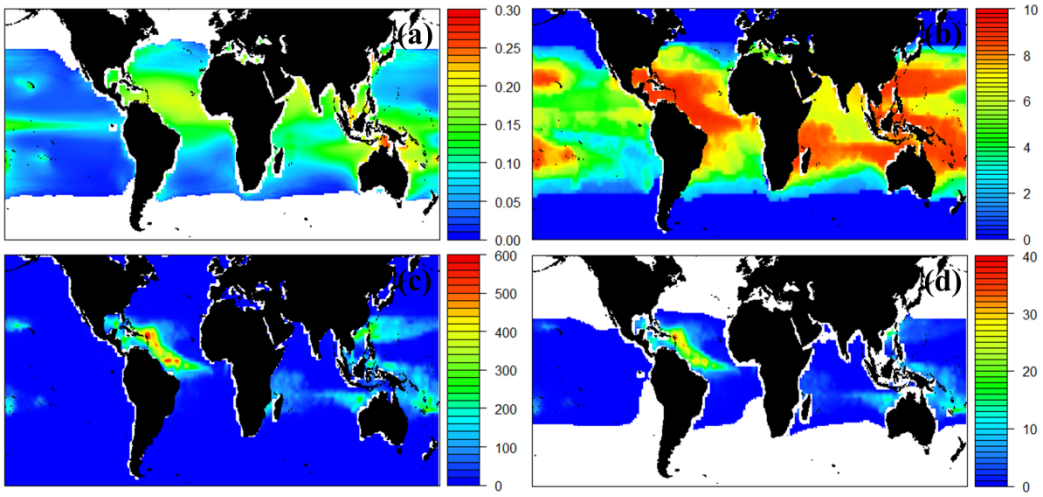


gcb_15324_f5.png